A theoretical and experimental study of the SO_2^{2+} dication

M. Hochlaf, and J. H. D. Eland

Citation: The Journal of Chemical Physics **120**, 6449 (2004); doi: 10.1063/1.1652544
View online: http://dx.doi.org/10.1063/1.1652544
View Table of Contents: http://aip.scitation.org/toc/jcp/120/14
Published by the American Institute of Physics

A theoretical and experimental study of the SO_2^{2+} dication

M. Hochlaf[a)]
Theoretical Chemistry Group, University of Marne-La-Vallée, Champs Sur Marne, F-77454, Marne-La-Vallée, cedex 2, France

J. H. D. Eland[b)]
Physical and Theoretical Chemistry Laboratory, Oxford University, OX1 3QZ, United Kingdom

(Received 12 December 2003; accepted 12 January 2004)

The double photoionization spectrum of SO_2 has been measured using the TOF–PEPECO technique and contains one resolved band. Detailed electronic structure calculations and experimental comparisons allow the resolved band to be identified as the $A\,^1A_2$ state of the SO_2^{2+} dication, with its adiabatic ionization energy at 35.284 ± 0.02 eV. According to the most accurate calculations, the ground state level of SO_2^{2+} must be located near 33.48 eV, well below the range accessed by vertical transitions from neutral SO_2. Transient SO_2^{2+} molecules detected by mass spectrometry may be identified either as the sharp levels of the $A\,^1A_2$ state or as ground state levels populated by nonvertical ionization pathways. © *2004 American Institute of Physics.*
[DOI: 10.1063/1.1652544]

I. INTRODUCTION

The SO_2^{2+} dication has never been detected as a stable species, but we can infer existence of a transient form with a lifetime of the order of 100 ns from observation of a metastable peak in the mass spectrum.[1] This paper presents vertical spectra of the doubly charged ion obtained by the TOF–PEPECO method, together with detailed interpretation using high level electronic structure calculations. A preliminary report of the spectrum has appeared.[2]

Previous knowledge of the SO_2^{2+} spectrum comes partly from studies of its dissociation pathways, initially by the PIPICO (photoion–photoion coincidence) technique,[3,4] then by triple coincidence PEPIPICO (photoelectron–PIPICO) without energy analysis of the electrons.[5,6] These measurements, together with a study of electron pair ion coincidences[7] and with threshold determinations from photoionization mass spectrometry[8] give the dication energy ranges for formation of each of the three charge separation exit channels:

$$SO^+ + O^+, \quad 34-38 \text{ eV},$$

$$S^+ + O_2^+, \quad 33-36 \text{ eV},$$

$$S^+ + O^+ + O, \quad >38 \text{ eV}.$$

The one charge-conserving dissociation channel leading to

$$SO^{2+} + O$$

apparently had a threshold around 35 eV. This value was refined as 35.8 ± 0.2 eV in the most recent study of the dissociation spectrum using PEPIPICO with energy analysis of one photoelectron.[9] The major conclusion of the work was that in all the above dissociation channels, the products are formed mainly in their ground states.

The classical route to the spectra of doubly charged ions is measurement of inner-shell Auger spectra. Oxygen and sulphur Auger spectra of SO_2 were measured by Thompson *et al.*[10] and have been interpreted using molecular orbital calculations on the doubly charged ion by Robb *et al.*[11]

The most direct previous study of the spectrum of SO_2^{2+} was made by the double charge transfer (DCT) technique. Using H^+, F^+, and OH^+ projectiles, Griffiths *et al.*[12] were able to obtain, separately, spectra of the singlet and triplet states of the dication in the 0–17 eV internal energy range. These spectra gave vertical ionization energies to many states with an apparent resolution of about 200 meV. The spectra were compared with theoretical calculations using the second-order Algebraic Diagrammatic Construction propagator method [ADC(2)].[12] Their calculated values were considered to be accurate to within 0.4 eV compared to their DCT double ionization energies. Earlier theoretical calculations of SO_2^{++} vertical excitation energies were also performed at the Hartree–Fock+CI (Ref. 11) and CIPSI levels of theory.[13] These predicted energies are significantly less accurate than the ADC(2) results.

The present calculations include not only the vertical energies but also the potential energy surfaces of SO_2^{++} ($X\,^1\Sigma_g^+, a\,^3B_2, A\,^1A_2$) and the resulting vibrational energy level manifolds. The ionization energies calculated by the highly correlated methods described below are expected to be significantly more accurate than previous calculations. We have also investigated the one-dimensional dissociation pathways leading to the lowest dissociation limits, involving the singlet and triplet electronic states of this dication. In light of these calculations, the metastability of the lowest electronic states of this dication is discussed.

II. EXPERIMENTAL METHOD

The basis of the TOF–PEPECO method is detection and energy analysis of both electrons of each pair ejected in

a)Electronic mail: hochlaf@univ-mlv.fr
b)Electronic mail: eland@physchem.ox.ac.uk

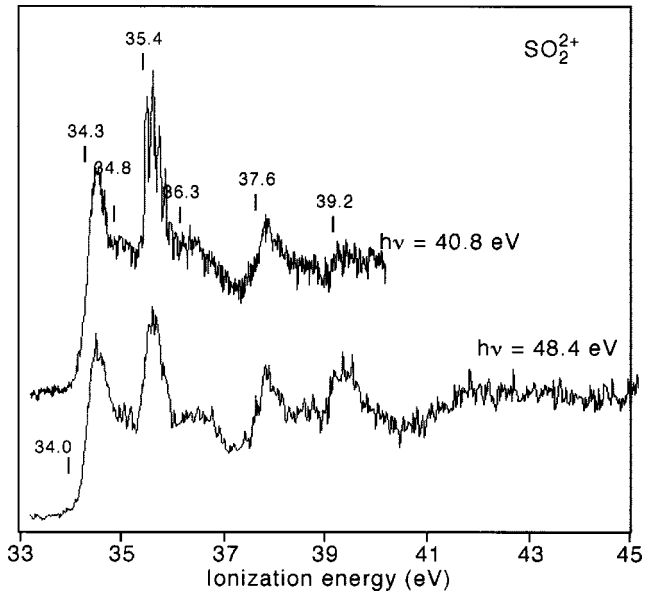

FIG. 1. Double photoionization spectra of SO_2 at the different wavelengths, with indications of the vertical double ionization energies.

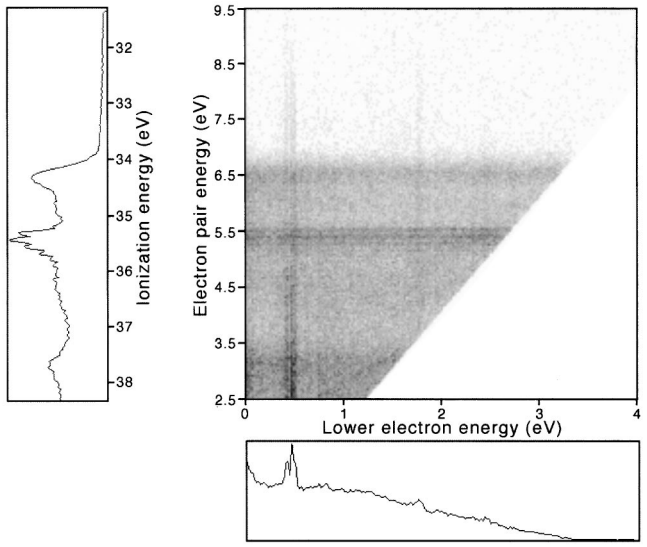

FIG. 3. Full electron pair energy distribution at 30.4 nm as a density map of the summed electron pair energy versus the lower of the two electron energies, with the double ionization spectrum and single electron energy distribution spectrum as projections.

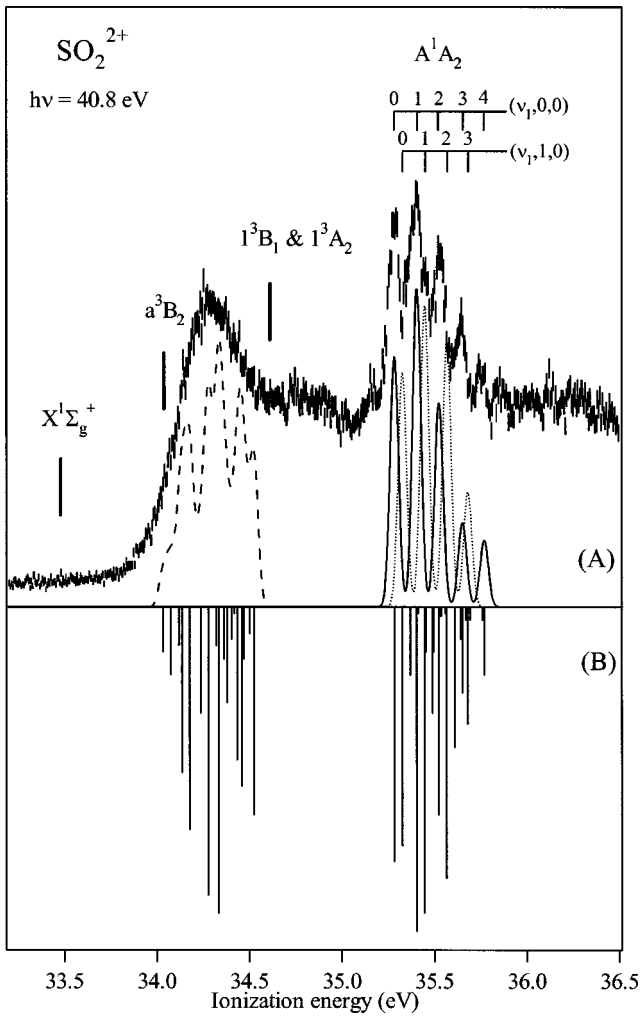

FIG. 2. Detail of the low energy part of the spectrum at 30.4 nm (A). In (B), the calculated FCFs are given. See text for more details.

double photoionization. The light source is a pulsed discharge lamp with helium or neon as the working gas; in its present form it gives ca. 5 ns pulses at 7 kHz repetition rate. Ionization occurs where wavelength selected light is focussed into an effusive gas jet at the focus of a long (5.5 m) magnetic bottle time-of-flight spectrometer. Further details have been given in previous papers.[2,14,15]

Double ionization spectra of SO_2 were accumulated at two wavelengths 30.4 and 25.6 nm. Calibration was by comparison with the 58.4 nm photoelectron spectrum of O_2, measured immediately before and after each run. Because the detection times of all electrons are recorded in list mode, contact potential changes during the long run times could be compensated in the data reduction. Spectra from each few hours of runtime were cross correlated and optimum shifts determined before addition to form the final spectra.

III. COMPUTATIONAL METHODS

The electronic structure calculations were performed using the complete active space self-consistent field (CASSCF)[16] and internally contracted multireference configuration interaction (MRCI) methods[17,18] or the coupled clusters approach with perturbative treatment of triple excitations (CCSD(T))[19] incorporated in the MOLPRO program suite.[20] Such highly correlated *ab initio* methods are needed in the calculations of the potential energy functions (PEFs) and the properties of dications since electronic correlations are expected to play an important role in their metastability. The generally contracted *spdf* cc-pVQZ basis set of Dunning has been used for S and O, resulting in 142 contracted Gaussian functions.[21] In this work, the C_2 axis of the C_{2v} point group is chosen to be the *y* axis for the symmetry designation of the electronic states.

The three-dimensional PEF of the $SO_2^{++}(X\,^1\Sigma_g^+)$ has

TABLE I. Dominant electronic configurations and CASSCF vertical excitation energies (T_e) of triplet and singlet states of SO_2^{++}.

Electronic state	Electronic configuration[a]	Theory			Experiment	
		T_e (eV)	T (eV)[b]	ADC(2)[c]	DCT[c]	Auger spectroscopy[d]
$1\,^1A_1$ $(X\,^1\Sigma_g^+)$[e]	$(8a_1)^{-2}$	34.23[h]	33.48[h]	34.3	34.5±0.2	34.5±0.3
$1\,^3B_2$[f]	$(5b_2)^{-1}(8a_1)^{-1}$	34.26	34.19	34.2	34.1±0.4	
$1\,^3B_1$	$(5b_2)^{-1}(1a_2)^{-1}$	36.02	34.71	36.0	36.2±0.2	
$1\,^3A_2$	$(1a_2)^{-1}(8a_1)^{-1}$	34.75	34.75	35.1	35.0±0.2	
$1\,^1A_2$[g]	$(1a_2)^{-1}(8a_1)^{-1}$	35.23	35.23		35.6±0.2	35.2±0.3
$1\,^1B_2$	$(5b_2)^{-1}(8a_1)^{-1}$	35.54	35.54	35.6		
$1\,^1B_1$	$(5b_2)^{-1}(1a_2)^{-1}$	36.29	35.92			
$2\,^1A_1$	$(5b_2)^{-2}$	36.49	36.19	36.6	36.6±0.3	36.6±0.3
$3\,^1A_1$	$(1a_2)^{-2}$	37.57	37.26	37.9	37.9±0.3	38.1±0.3
$2\,^3B_1$	$(2b_1)^{-1}(8a_1)^{-1}$	37.79	37.62			
$1\,^3A_1$	$(7a_1)^{-1}(8a_1)^{-1}$	37.77	37.67	37.8	37.6±0.2	
$2\,^3B_2$	$(4b_2)^{-1}(8a_1)^{-1}$	37.92	37.88	38.5	38.6±0.2	
$2\,^1A_2$	$(5b_2)^{-1}(2b_1)^{-1}$	38.36	38.12	38.8	38.7±0.3	38.8±0.3
$2\,^3A_2$	$(2b_1)^{-1}(5b_2)^{-1}$	38.66	38.35			
$2\,^1B_1$	$(2b_1)^{-1}(8a_1)^{-1}$	38.71	38.7			
$3\,^3B_2$	$(5b_2)^{-1}(7a_1)^{-1}$	38.7	38.71			
$4\,^3B_2$	$(2b_1)^{-1}(1a_2)^{-1}$	38.87	38.77	39.4	39.5±0.3	
$2\,^3A_1$	$(4b_2)^{-1}(5b_2)^{-1}$	39.13	38.78			
$3\,^3B_1$	$(4b_2)^{-1}(1a_2)^{-1}$	39.53	39.23			
$2\,^1B_2$	$(4b_2)^{-1}(8a_1)^{-1}$	39.48	39.28			
$4\,^1A_1$	$(7a_1)^{-1}(8a_1)^{-1}$	39.44	39.36	39.5	39.7±0.3	39.7±0.3
$3\,^3A_2$	$(8a_1)^{-2}(5b_2)^{-1}(3b_1)^{+1}$	39.42	39.39	40.4	40.5±0.3	
$3\,^1A_2$	$(8a_1)^{-2}(5b_2)^{-1}(3b_1)^{+1}$	39.67	39.6			
$4\,^3B_1$	$(8a_1)^{-1}(5b_2)^{-2}(3b_1)^{+1}$	40.45	39.97			
$4\,^3A_2$	$(1a_2)^{-1}(7a_1)^{-1}$	40.2	40.07			
$3\,^3A_1$	$(8a_1)^{-1}(5b_2)^{-1}(1a_2)^{-1}(3b_1)^{+1}$	40.12	40.09			
$4\,^3A_1$	$(8a_1)^{-1}(5b_2)^{-1}(1a_2)^{-1}(3b_1)^{+1}$	41.05	40.73	41.8	41.4±0.3	
$3\,^1B_2$	$(5b_2)^{-1}(7a_1)^{-1}$	41.72	40.95	41.5	41.4±0.3	41.5±0.3
$3\,^1B_1$	$(4b_2)^{-1}(1a_2)^{-1}$	41.44	41.16			
$4\,^1A_2$	$(7a_1)^{-1}(1a_2)^{-1}$	41.65	41.36			
$4\,^1B_1$	$(8a_1)^{-1}(5b_2)^{-2}(3b_1)^{+1}$	41.83	41.5			
$4\,^1B_2$	$(5b_2)^{-1}(6a_1)^{-1}$	42.2	42.19			

[a]Electronic configuration of SO_2 $(X\,^1A_1)$: $(1a_1)^2(2a_1)^2(1b_2)^2(3a_1)^2(4a_1)^2(2b_2)^2(1b_1)^2(5a_1)^2(3b_2)^2(6a_1)^2(7a_1)^2(4b_2)^2(2b_1)^2(5b_2)^2(1a_2)^2(8a_1)^2$.

[b]Difference between the CASSCF energies at the equilibrium geometry of SO_2^{++} $(X\,^1\Sigma_g^+)$ and at the equilibrium geometry of the corresponding electronic state.

[c]Reference 12.

[d]Reference 10.

[e]Corresponds to $X\,^1\Sigma_g^+$ state of SO_2^{++}.

[f]Labeled as $a\,^3B_2$ in the other tables.

[g]Labeled as $A\,^1A_2$ in the other tables.

[h]Total CASSCF energy at the equilibrium geometry of SO_2^{++} $(X\,^1\Sigma_g^+)$ state: −546.306 737 a.u. We have added 33.48 eV corresponding to the new double ionization potential found here for SO_2 (see text).

been mapped in C_s symmetry, using the CCSD(T) approach. The calculations were performed for 22 different geometries covering the region up to 5000 cm^{-1} above the equilibrium minimum of this state. For the SO_2^{++} $(a\,^3B_2, A\,^1A_2)$, the PEFs have been generated using the CASSCF and MRCI methods. In order to reduce symmetry breaking problems, the CASSCF computations started with the HF molecular orbitals obtained for $SO_2(X\,^1A_1)$. In the active space all valence molecular orbitals were optimized. For MRCI calculations, all configurations with coefficients larger than 0.005 in the CI expansion of the CASSCF wave functions were taken into account as a reference. All valence electrons were correlated. The calculations were done in C_s symmetry with wave functions corresponding to more than 350×10^6 uncontracted configurations. The PEFs have been mapped for 35 different geometries around the equilibrium minima of these electronic states covering the energies up to 8000 cm^{-1}. For the SO_2^{++} $(a\,^3B_2)$, the MRCI energies including Davidson corrections were considered in the aim to get more accurate results.

The one-dimensional PEFs of the lowest singlet and triplet electronic states of SO_2^{++} have been calculated at the CASSCF level of theory, using a similar approach as described above for SO_2^{++} $(a\,^3B_2, A\,^1A_2)$. In these calcula-

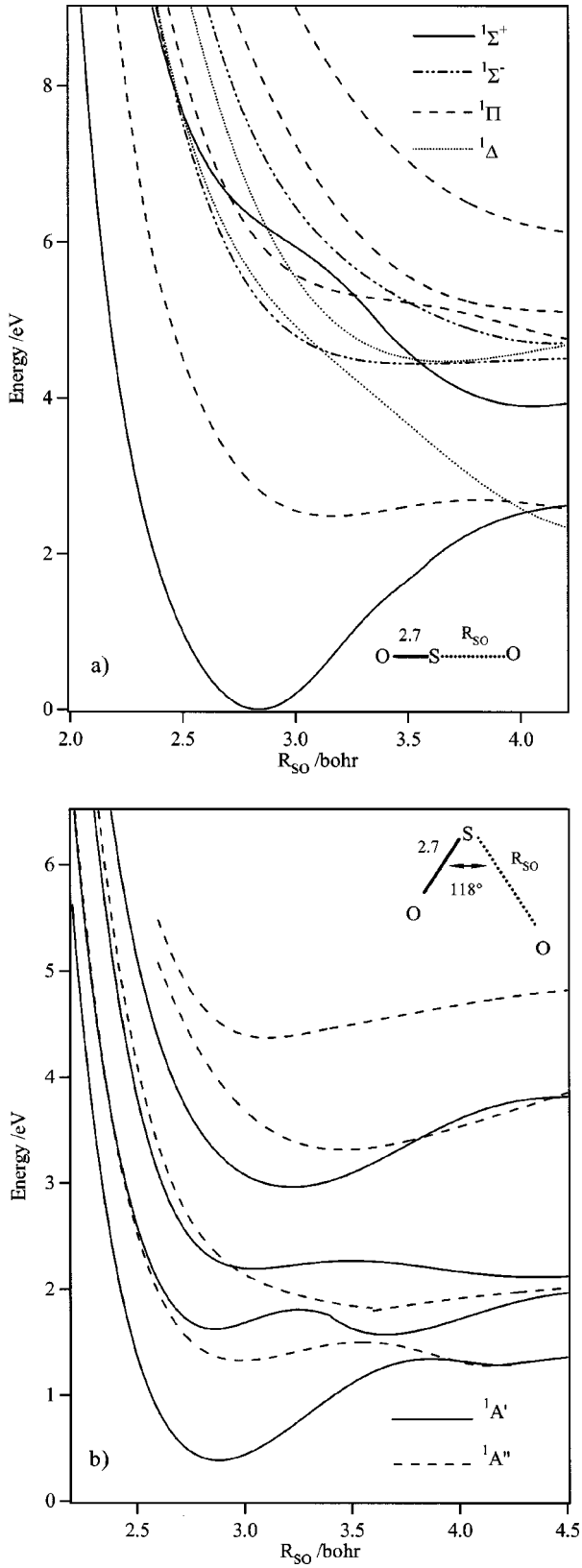

FIG. 4. CASSCF potential energy curves of the singlet states of SO_2^{++} for linear (a) and bent (b) structure (θ=118°) of the dication. The other R_{SO} distance is kept fixed at 2.7 bohr.

tions, all electronic states with the same spin multiplicity have been averaged together. The spin–orbit couplings in Cartesian coordinates have been evaluated over the CASSCF wave functions at the crossings between some electronic

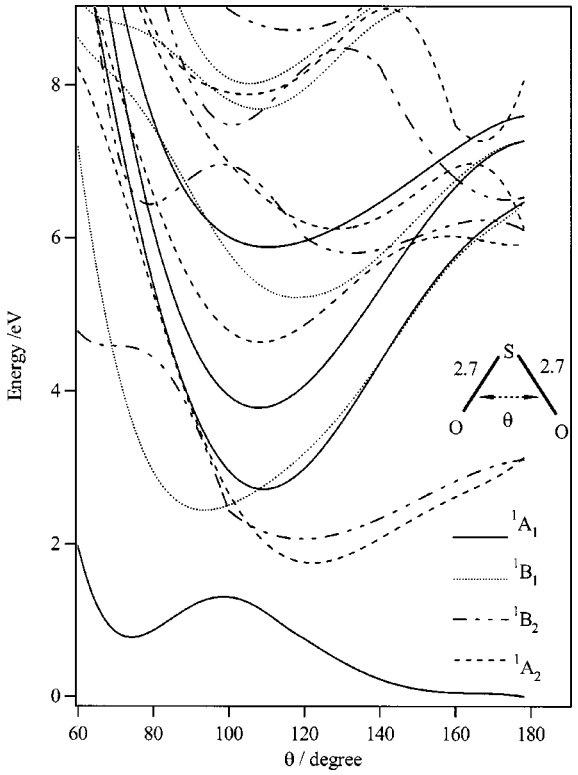

FIG. 5. CASSCF potential energy curves of the singlet states of SO_2^{++} vs the bending angle θ. Both R_{SO} distances are kept fixed at 2.7 bohr.

SO_2^{++} states which are expected to play a role in the metastability of this dication (see below). The accuracy of the spin–orbit calculations is assumed to be better than 5% compared to experimental values for triatomic molecular systems.[22–24]

For the SO_2^{++} ($X\,^1\Sigma_g^+$, $a\,^3B_2$, $A\,^1A_2$) states, the calculated energies were fitted to polynomial expansions in displacement coordinates corresponding to $R_{1,2}$ (R_{SO}, sulfur–oxygen distance) and θ (OSO bending angle). The resulting PEF expansions were used to calculate the quartic force fields in internal coordinates, which have been transformed by the *l*-tensor algebra to the quartic force fields in dimensionless normal coordinates.[25,26] These data allow us to evaluate a set of spectroscopic properties using second order perturbation theory. The PEF expansions were also used in variational calculations, where the full dimensionality and all anharmonic and angular momentum coupling effects were taken into consideration.[27] For similar calculations of other triatomic dications, readers are referred to Refs. 28 and 29.

As part of this work, the three-dimensional PEF of the ground state $X\,^1A_1$ of SO_2 has been generated at the CCSD(T) level of theory. These calculations are not presented here. The calculated fundamentals differ by less than 10 cm^{-1} from the experimental values.[30] This PEF can be sent when requested. This PEF has been used to evaluate the Franck–Condon factors (presented in Sec. IV C) corresponding to the direct double photoionization process.

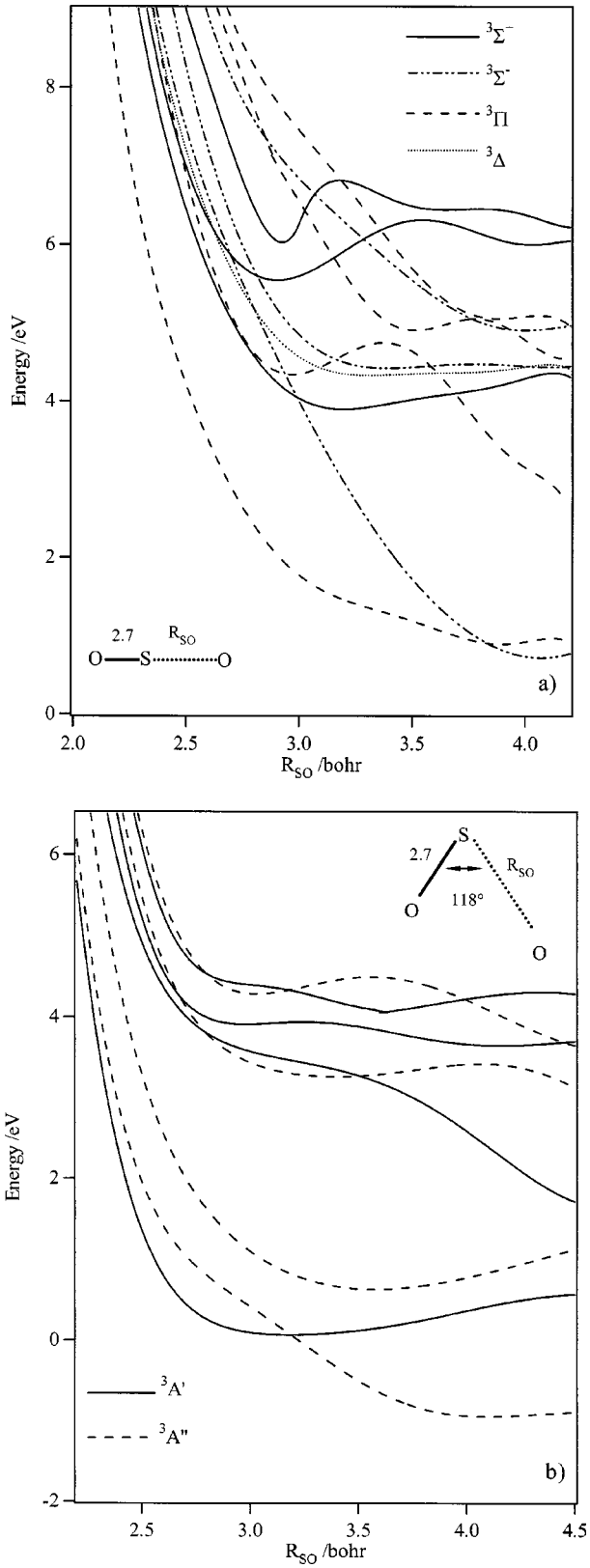

FIG. 6. CASSCF potential energy curves of the triplet states of SO_2^{++} for linear (a) and bent (b) structures (θ=118°) of the dication. The other R_{SO} distance is kept fixed at 2.7 bohr.

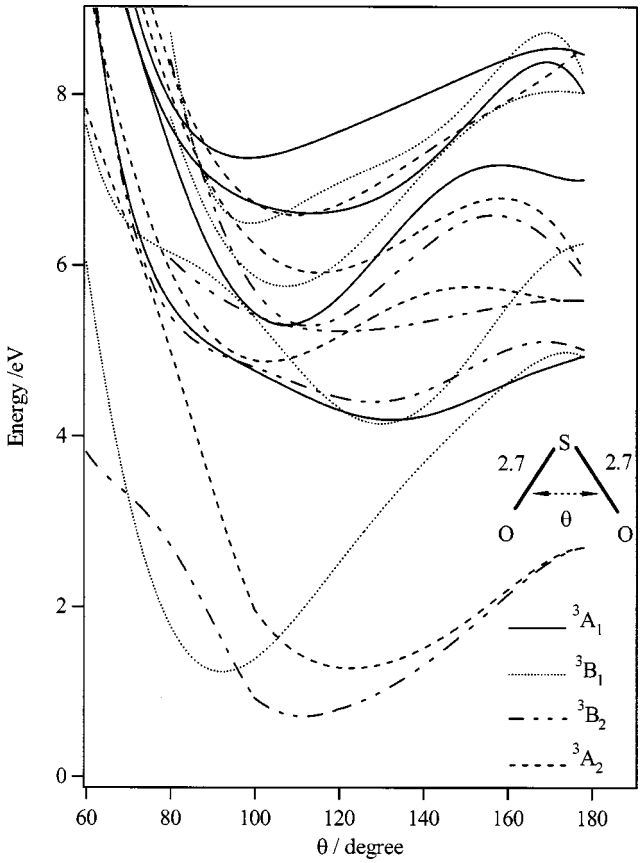

FIG. 7. CASSCF potential energy curves of the triplet states of SO_2^{++} vs the bending angle θ. Both R_{SO} distances are kept fixed at 2.7 bohr.

IV. RESULTS

A. Experimental spectra

Figure 1 shows the double photoionization spectra of SO_2 at the different wavelengths. The onset of significant intensity is at about 34.0 eV and at higher energies six distinct bands can be recognized, one (the third, at 35.4 eV) showing vibrational structure. The position of this band, indicated as a vertical ionization energy in Fig. 1, agrees closely with the second singlet state band (35.6±0.2 eV, *B*) from the DCT results[12] which was attributed there to either $^1B_2$ or $^1A_2$. Other agreements can be recognized between the first band at 34.3 eV and the first triplet DCT band (34.3 eV) and between the 35.0 eV feature and the second DCT triplet band (35.0 eV). For the other bands noted in Fig. 1 both singlet and triplet bands at closely corresponding energies can be found in the DCT results, so no clear spin attribution can be made. Figure 2 shows details of the low energy part of the spectrum at 30.4 nm, including the resolved band. There seems to be a progression with intervals of about 120 meV (970 cm^{-1}) showing some anharmonicity. Weak extra peaks are seen 120 meV before the first strong peak and 50 meV above the second peak. The peak widths also vary, suggesting that there may be underlying unresolved structure present. The absolute position of the first strong peak in the resolved band is 35.284 eV with an uncertainty estimated as of ±0.02 eV; the uncertainty derives mainly from the calibration method, and spacings within the resolved structure are more accurate. Figure 3 shows the full electron pair energy distribution at 30.4 nm as a density map of the summed electron pair energy versus the lower of the two electron energies, with the double ionization spectrum and single electron energy distribution spectrum as projections. The

TABLE II. Quartic force fields in dimensionless normal coordinates of SO_2^{++} ($X\ ^1\Sigma_g^+$, $a\ ^3B_2$, and $A\ ^1A_2$) states. All values are in cm^{-1}.

	$X\ ^1\Sigma_g^+$	$a\ ^3B_2$	$A\ ^1A_2$
ω_1	1009.5	866.4	1025.0
ω_2	228.6	345.0	360.9
ω_3	1459.2	654.4	731.4
ϕ_{111}	−282.7	−298.1	−167.4
ϕ_{222}		−41.2	34.7
ϕ_{112}		−17.4	−47.8
ϕ_{122}	149.4	22.6	46.8
ϕ_{133}	−402.0	−375.2	−452.3
ϕ_{233}		−32.6	16.7
ϕ_{1111}	56.7	51.5	31.1
ϕ_{2222}	78.2	−0.1	−41.5
ϕ_{3333}	107.0	87.8	248.7
ϕ_{1122}	−58.4	−13.6	−19.9
ϕ_{2233}	−100.5	−28.8	−40.0
ϕ_{1133}	79.0	97.2	41.8
ϕ_{1222}		2.5	−8.1
ϕ_{1233}		−8.9	1.4
ϕ_{1112}		10.1	6.7

map and its projections show that in addition to molecular double ionization, a dissociative double ionization exists with the following steps:

$$SO_2 + h\nu \rightarrow SO_2^{+}{}^* + e^- : SO_2^{+}{}^* \rightarrow SO^+ + O^* : O^*$$
$$\rightarrow O^+ + e^-.$$

The same process, involving the same autoionizing levels of O* has been recognized before in double ionization of O_2, CO, NO, CO_2 and also a similar process in H_2S.[31] This dissociative process extends below the molecular double ionization potential of SO_2, and may have caused difficulty in previous experimental estimates of the molecular double ionization threshold.

Apart from the atomic autoionization lines, the two-dimensional electron pair energy distribution is rather flat and featureless, suggesting that molecular autoionization processes play only a minor role and that the double ionization is mainly direct. The featureless distribution may, however, arise in this case from overlap of multiple unresolved bands.

B. On the excited states of SO_2^{++}

Table I lists the dominant electronic configurations, the calculated vertical transitions energies (T) at CASSCF and ADC(2)[12] levels of theory and measured using the DCT[12] and Auger spectroscopy[10] techniques. This dication presents a high density of electronic states even for internal energies as low as 5 eV. Below this energy, the electronic configurations of the electronic states correspond mostly to the removal of two electrons from the valence orbitals. For higher energies, the removal of the two electrons from valence orbitals is accompanied by simultaneous excitation of a third one into the vacant ($3b_1$) orbital during the double ionization process. The assignment of the experimental bands shown in this work and in the DCT experiments[12] in terms of the electronic states depends on our identification of the resolved band, for which a precise adiabatic ionization energy can be determined, as the $1\ ^1A_2$ state. The arguments for this assignment are detailed below.

TABLE III. MRCI adiabatic excitation energies (T_0), equilibrium geometries, rotational constants (A_e, B_e, C_e, and α), l-doubling constant (q), anharmonic vibrational constants (x,g_{22}) and zero point vibrational energies of SO_2^{++} ($X\ ^1\Sigma_g^+$, $a\ ^3B_2$, and $A\ ^1A_2$) states. All values are in cm^{-1} except if specified.

	$X\ ^1\Sigma_g^+$	$a\ ^3B_2$	$A\ ^1A_2$
T_0 (eV)	0[a]	0.554[a]	1.805[a]
R_e (bohr)	2.683	2.893	2.840
θ_e=OSO angle (degree)	180°	108.2	123.4
A_e		1.309	2.077
B_e	0.261	0.342	0.301
C_e		0.271	0.263
$\alpha_e^{1,A}$		0.0071	−0.019
$\alpha_e^{2,A}$		−0.0271	−0.032
$\alpha_e^{3,A}$		0.0101	0.038
$\alpha_e^{1,B}$	0.001 26	0.0025	0.0015
$\alpha_e^{2,B}$	−0.000 55	0.0001	−0.0015
$\alpha_e^{3,B}$	0.002 08	0.0031	0.0015
$\alpha_e^{1,C}$		0.0018	0.0008
$\alpha_e^{2,C}$		0.0010	0.0002
$\alpha_e^{3,C}$		0.0022	0.0017
q	0.000 65		
x_{11}	−4.7	−7.5	−1.7
x_{12}	−1.0	−1.7	−1.4
x_{13}	−24.1	−56.2	−76.1
x_{22}	0.39	−0.7	−3.4
x_{23}	−8.5	−5.3	−4.7
x_{33}	−11.9	−7.2	2.5
g_{22}	0.108		
$G(0,0,0)$[b]	1451	919	1049

[a]Total MRCI energy at the equilibrium geometry of SO_2^{++} ($X\ ^1\Sigma_g^+$) state: −546.766 513 68 a.u.
[b]Calculated variationally.

The CASSCF one-dimensional cuts of the potential energy functions of the lowest singlet states of SO_2^{++} for linear and bent structures (θ=118°) are presented in Figs. 4(a) and 4(b), respectively. In these calculations, we have varied one SO distance (R_{SO}) and the other SO distance is kept fixed at 2.7 bohr. These potential energy curves are given relative to the energy of the equilibrium geometry of SO_2^{++} ($X\ ^1\Sigma_g^+$). Figure 5 presents the singlet electronic states versus the OSO bending angle (θ). These curves have been obtained by fixing both R_{SO} distances to 2.7 bohr and by varying θ. Figure 5 shows that, except the electronic ground state $X\ ^1\Sigma_g^+$, all the excited states have bent structures. Moreover the lowest $^1A_2$ and $^1B_2$ states correlate to the same $^1\Pi_g$ state at linearity corresponding so to the well-known Renner–Teller effect. The second $^1A_1$ and the first $^1B_1$ states (as well as the third $^1A_1$ and the second $^1B_1$ states) correlate to a $^1\Pi_u$ state at linearity. Singlet states also exhibit several avoided crossings for both linear and bent configurations. For example, we notice one between the two lowest $^1A_1$ states (cf. Fig. 5) at $\theta \sim 105°$, which is responsible for the local minimum in the lower state at $\theta \sim 75°$ [located at ~0.77 eV above the equilibrium geometry of SO_2^{++} ($X\ ^1\Sigma_g^+$) and separated by a barrier of ~0.5 eV]. In addition, some conical intersections can be found for these singlet states. For instance, we can cite

TABLE IV. Rovibrational levels of SO_2^{++} ($X\ ^1\Sigma_g^+$).

$J=0$				$J=1$			
σ_g^+		σ_u^+		π_u		π_g	
(v_1,v_2,v_3)	Energy (cm^{-1})	(v_1,v_2,v_3)	Energy (cm^{-1})	(v_1,v_2,v_3)	Energy (cm^{-1})	(v_1,v_2,v_3)	Energy (cm^{-1})
(0,0,0)	0	(0,0,1)	1416	(0,1,0)	225	(0,1,1)	1633
(0,2,0)	451	(0,2,1)	1850	(0,3,0)	677	(0,3,1)	2068
(0,4,0)	904	(0,4,1)	2287	(0,5,0)	1132	(0,5,1)	2507
(1,0,0)	988	(1,0,1)	2384	(1,1,0)	1212	(1,1,1)	2599
(0,6,0)	1361	(0,6,1)	2727	(0,7,0)	1591	(0,7,1)	2949
(1,2,0)	1437	(1,2,1)	2816	(1,3,0)	1662	(1,3,1)	3033
(0,8,0)	1820	(0,8,1)	3171	(0,9,0)	2051	(0,9,1)	3393
(1,4,0)	1888	(1,4,1)	3251	(1,5,0)	2115	(1,5,1)	3469
(2,0,0)	1968	(2,0,1)	3346	(2,1,0)	2191	(2,1,1)	3561
(0,10,0)	2282	(0,10,1)	3617	(0,11,0)	2514	(0,11,1)	3841
(1,6,0)	2343	(1,6,1)	3689	(1,7,0)	2571	(1,7,1)	3909
(2,2,0)	2415	(2,2,1)	3776	(2,3,0)	2639	(2,3,1)	3992
(0,12,0)	2746			(0,13,0)	2979		
(1,8,0)	2800			(0,1,2)	3020		
(0,0,2)	2812			(1,9,0)	3029		
(2,4,0)	2864			(2,5,0)	3090		
(3,0,0)	2941			(3,1,0)	3163		
(0,14,0)	3213			(0,3,2)	3438		
(0,2,2)	3229			(0,15,0)	3447		
(1,10,0)	3259			(1,11,0)	3490		
(2,6,0)	3317			(2,7,0)	3544		
(3,2,0)	3385			(3,3,0)	3609		
(0,4,2)	3649			(0,5,2)	3861		
(0,16,0)	3681			(0,17,0)	3917		
(1,12,0)	3721			(1,13,0)	3953		
(1,0,2)	3763			(1,1,2)	3970		
(2,8,0)	3771						
(3,4,0)	3833						
(4,0,0)	3906						

one between the two lowest $^1A_2$ and $^1B_1$ states for $\theta\sim100°$ (cf. Fig. 5). For the linear configuration we also notice a conical intersection between the second $^1\Pi$ and the second $^1\Sigma^+$ states at $R_{SO}\sim3.25$ bohr [cf. Fig. 4(a)]. Hence in C_s symmetry, the two $^1A'$ components will form an avoided crossing and the two states will be coupled by the bending and the antisymmetric stretching modes.

Figures 6(a), 6(b), and 7 present similar calculations for the triplet states of SO_2^{++}. These triplets exhibit, like the singlets, several avoided crossings [for example, those involving the $^3\Sigma^+$ states, cf. Fig. 6(a)], conical intersections and Renner–Teller interactions (for instance between the lowest $^3A_2$ and $^3B_2$, cf. Fig. 7). Specifically, we draw attention to the conical intersection between the lowest $^3A_2$ and $^3B_1$ states for $\theta\sim105°$ (cf. Fig. 7). The crossing between these two electronic states is located close to the equilibrium geometries of these electronic states (less than 0.4 eV above their equilibrium minima). Such an interaction strongly disturbs the rovibronic structure of these electronic states so that we cannot treat each electronic state separately, but a full treatment is not done in the present work. Moreover, the lowest $^3\Sigma^-$ [$^3A''$ in Fig. 6(b)] is found to be repulsive in nature. It crosses all the other electronic states. It correlates to the $SO^+(X\ ^2\Pi)+O^+(^2D)$ limit which is located below several electronic states of this dication, thus, it may play a role in their predissociation, though experiments show that most dissociation goes to the lowest asymptote $SO^+(X\ ^2\Pi)+O^+(^4S)$.

Our identification of the resolved spectral band at 35.4 eV as the $A\ ^1A_2$ state is based on three main arguments: First, the experimental agreement of its energy with a singlet DCT band[12] establishes the multiplicity; the energy compared with the present and previous calculations then leaves only the $A\ ^1A_2$ and $1\ ^1B_2$ states as possibilities. Second, the accuracy of relative energies in the present calculations is ±0.1 eV or better; when we identify the 35.4 eV state as $A\ ^1A_2$, all the peaks in Fig. 1 and at least five DCT bands[12] can be assigned and agree in position to about this accuracy. If the identification is made with $1\ ^1B_2$, the agreement is significantly worse. Third, the shape of the resolved band agrees well with the Franck–Condon calculation as shown in Fig. 2. Because the potential energy surface for $1\ ^1B_2$ is markedly different, no similar agreement can be expected with the alternative identification. In view of this identification we have carried out more detailed calculations on three states.

C. Potential energy functions, spectroscopic constants and rovibronic structure of SO_2^{++} ($X\ ^1\Sigma_g^+$, $a\ ^3B_2$, and $A\ ^1A_2$) states

The lowest $^3A_2$ and $^3B_2$ states correlate to the same $^3\Pi_g$ state at linearity so forming a Renner–Teller system (see Fig.

TABLE V. Rovibrational levels of SO_2^{++} ($a\ ^3B_2$) and calculated Franck–Condon factors (FCF).

(v_1,v_2,v_3)	Energy (cm^{-1})	FCF[a]	(v_1,v_2,v_3)	Energy (cm^{-1})	FCF[a]	(v_1,v_2,v_3)	Energy (cm^{-1})	(v_1,v_2,v_3)	Energy (cm^{-1})
(0,0,0)	0	1.69	(2,1,2)	2889		(0,0,1)	609	(2,0,3)	3081
(0,1,0)	340	2.56	(2,4,0)	2984	1.21	(0,1,1)	943	(2,3,1)	3113
(0,2,0)	679	1.44	(0,9,0)	3008		(0,2,1)	1275	(3,1,1)	3188
(1,0,0)	821	6.25	(1,3,2)	3029		(1,0,1)	1373	(0,8,1)	3229
(0,3,0)	1016		(3,2,0)	3103	0.25	(0,3,1)	1605	(0,1,5)	3233
(1,1,0)	1155	8.41	(0,6,2)	3108		(1,1,1)	1697	(1,2,3)	3289
(0,0,2)	1209		(0,4,2)	3135		(0,0,3)	1800	(1,6,1)	3299
(0,4,0)	1351		(1,7,0)	3187		(0,4,1)	1933	(2,1,3)	3381
(1,2,0)	1487		(2,2,2)	3211		(1,2,1)	2019	(0,5,3)	3399
(0,1,2)	1541		(4,0,0)	3221	5.76	(0,1,3)	2123	(2,4,1)	3436
(2,0,0)	1629	4.00	(1,4,2)	3307		(2,0,1)	2143	(1,3,3)	3519
(0,5,0)	1686		(2,5,0)	3318		(0,5,1)	2260	(0,9,1)	3548
(1,3,0)	1817		(0,10,0)	3334		(1,3,1)	2339	(3,2,1)	3563
(0,2,2)	1871		(1,0,4)	3366		(0,2,3)	2443	(0,6,3)	3604
(1,0,2)	1926		(3,0,2)	3426		(1,0,3)	2465	(0,4,3)	3647
(2,1,0)	1973	10.89	(3,3,0)	3441	6.76	(2,1,1)	2524	(1,7,1)	3717
(0,6,0)	2018		(0,7,2)	3486		(0,6,1)	2585	(2,2,3)	3724
(1,4,0)	2143		(1,8,0)	3513		(1,4,1)	2657	(4,0,1)	3758
(0,3,2)	2201		(0,3,4)	3526		(0,3,3)	2762	(1,4,3)	3770
(1,1,2)	2246		(4,1,0)	3533	1.96	(1,1,3)	2789	(2,5,1)	3848
(2,2,0)	2312	1.44	(0,0,6)	3593		(1,1,3)	2857	(0,10,1)	3864
(0,7,0)	2350		(1,5,2)	3652		(0,7,1)	2908	(1,0,5)	3876
(0,0,4)	2424		(0,11,0)	3660		(2,2,1)	2912	(3,0,3)	3897
(3,0,0)	2434	11.56	(2,6,0)	3704		(0,0,5)	2974	(3,3,1)	3917
(1,5,0)	2467		(0,8,2)	3718		(0,4,3)	3041	(0,7,3)	3994
(0,4,2)	2531		(3,1,2)	3742					
(2,0,2)	2567		(3,4,0)	3778	1.00				
(2,3,0)	2649	1.96	(1,1,4)	3837					
(1,2,2)	2679		(1,9,0)	3839					
(0,8,0)	2697		(0,4,4)	3856					
(0,1,4)	2763		(0,1,6)	3922					
(3,1,0)	2785	3.61	(5,0,0)	3960	7.84				
(1,6,0)	2789		(1,6,2)	3985					
(0,5,2)	2860		(0,12,0)	3986					

[a]Only the contributions $\geqslant 0.25$ are given here.

7). Since the barriers to linearity of both components are quite high (more than 1 eV) and for such a heavy atom molecule, such an effect will not affect their lowest rovibrational levels, which are of interest in the present spectroscopic studies. Hence, each Renner–Teller component will be treated separately for its spectroscopy. Similarly, the lowest $^1A_2$ and $^1B_2$ states correlate to the same $^1\Pi_g$ state at linearity forming a bent/bent Renner–Teller system. Here again, the barriers to linearity of each component are high enough (more than 1 eV) so that the Renner–Teller interaction can be neglected for the lowest rovibrational levels of $^1A_2$. Although the $^3B_1$ and $^3A_2$ states lie in energy between the $a\ ^3B_2$ and the $A\ ^1A_2$ states, their PEFs are not generated in the present work, because of the conical intersection emphasized in the preceding section.

The quartic force fields in dimensionless normal coordinates of SO_2^{++} ($X\ ^1\Sigma_g^+$, $a\ ^3B_2$ and $A\ ^1A_2$) states are given in Table II. The relatively large values for the term Φ_{133} is indicative of strong anharmonic couplings between the ν_1 and ν_3 modes. Moreover, the ground state presents a large value for the term Φ_{122} due to strong anharmonic couplings between the ν_1 and ν_2 modes. The quartic force fields of Table II have been used to deduce a set of spectroscopic constants for SO_2^{++} ($X\ ^1\Sigma_g^+$, $a\ ^3B_2$, and $A\ ^1A_2$) which are presented in Table III. They consist of MRCI adiabatic excitation energies (T_0), equilibrium geometries, rotational constants (A_e, B_e, C_e, and α), l-doubling constant (q), anharmonic vibrational constants (x,g_{22}) and zero point vibrational energies. The removal of two electrons from the highest occupied orbital ($8a_1$) of SO_2 is accompanied by a strong change in geometry from bent ($\theta_e = 119.5°$ for $SO_2\ X\ ^1A_1$) to linear configuration, forming so the SO_2^{++} ($X\ ^1\Sigma_g^+$) dicationic state. This transition is associated with a slight change in the R_{SO} distances which are calculated to be 1.42 Å for SO_2^{++} ($X\ ^1\Sigma_g^+$) and measured to be 1.432 Å for $SO_2\ X\ ^1A_1$.[30] By contrast, the SO_2^{++} ($a\ ^3B_2$ and $A\ ^1A_2$) excited states have bent structures ($\theta_e = 108.2°$ and 123.4°, respectively) and much longer R_{SO} distances (1.53 Å and 1.50 Å, respectively).

Tables IV, V, and VI present the rovibrational structures of SO_2^{++} ($X\ ^1\Sigma_g^+$, $a\ ^3B_2$, and $A\ ^1A_2$), respectively, calculated using a variational approach. Levels higher than 2000 cm^{-1} are assigned tentatively because of anharmonic resonances. For the SO_2^{++} ($X\ ^1\Sigma_g^+$) state, the harmonic wave number of the bending mode (ω_2) is relatively low (228.6 cm^{-1}) and its x_{22} anharmonic vibrational constant is found to be slightly positive, signature of the inverse anharmonicity

TABLE VI. Rovibrational levels of SO_2^{++} (A^1A_2) and calculated Franck Condon factors (FCF).

(v_1,v_2,v_3)	Energy (cm^{-1})	FCF[a]	(v_1,v_2,v_3)	Energy (cm^{-1})	FCF[a]	(v_1,v_2,v_3)	Energy (cm^{-1})	(v_1,v_2,v_3)	Energy (cm^{-1})
(0,0,0)	0	9.61	(3,0,0)	2966	3.24	(0,0,1)	695	(1,1,3)	3121
(0,1,0)	351	9.00	(1,6,0)	2995		(0,1,1)	1041	(2,2,1)	3200
(0,2,0)	697	2.56	(0,9,0)	3051		(0,2,1)	1381	(1,5,1)	3237
(1,0,0)	978	12.25	(0,5,2)	3061		(1,0,1)	1587	(0,8,1)	3326
(0,3,0)	1038	0.25	(2,0,2)	3115	0.49	(0,3,1)	1716	(0,4,3)	3365
(1,1,0)	1325	11.56	(0,1,4)	3121		(1,1,1)	1927	(0,0,5)	3400
(0,4,0)	1375	1.69	(3,1,0)	3200	4.41	(0,4,1)	2048	(2,3,1)	3441
(0,0,2)	1393		(1,3,2)	3234		(0,0,3)	2085	(1,2,3)	3520
(1,2,0)	1667	4.00	(2,4,0)	3300	0.49	(1,2,1)	2261	(1,6,1)	3531
(0,5,0)	1710	1.69	(1,7,0)	3324		(0,5,1)	2377	(3,0,1)	3559
(0,1,2)	1736		(0,6,2)	3387		(2,0,1)	2421	(0,9,1)	3654
(2,0,0)	1940	7.84	(0,10,0)	3393		(0,1,3)	2467	(0,5,3)	3698
(1,3,0)	2003	0.36	(0,2,4)	3449		(1,3,1)	2589	(2,0,3)	3720
(0,6,0)	2044	0.36	(2,1,2)	3454		(0,6,1)	2706	(0,1,5)	3757
(0,2,2)	2073		(1,4,2)	3521		(0,2,3)	2752	(3,1,1)	3758
(1,0,2)	2217	0.25	(3,2,0)	3577		(1,0,3)	2796	(1,3,3)	3856
(2,1,0)	2288	10.24	(1,0,4)	3629		(2,1,1)	2864	(2,4,1)	3861
(1,4,0)	2336		(2,5,0)	3634		(1,4,1)	2914	(1,7,1)	3882
(0,7,0)	2378		(1,8,0)	3654		(0,7,1)	3035	(0,6,3)	3978
(0,3,2)	2405		(0,7,2)	3715		(0,3,3)	3078		
(1,1,2)	2549		(0,11,0)	3737					
(2,2,0)	2630	5.29	(1,5,2)	3780					
(1,5,0)	2666		(2,2,2)	3783					
(0,8,0)	2713		(0,3,4)	3802					
(0,4,2)	2734		(3,3,0)	3841	0.49				
(0,0,4)	2784		(4,0,0)	3915	2.56				
(1,2,2)	2876		(2,6,0)	3958					
(2,3,0)	2888	1.21	(1,9,0)	3986					

[a]Only the contributions $\geqslant 0.25$ are given here.

observed in the pattern of the bending levels. Such an effect is related to the flatness of the SO_2^{++} ($X\,^1\Sigma_g^+$) PEF relative to the bending coordinate, which is found to be less and less pronounced on increasing the electronic correlation level [from CASSCF, to MRCI, to CCSD(T)]. Tables V and VI list also the Franck–Condon factors (FCF) corresponding to direct double ionization from the neutral SO_2 ground state. For SO_2^{++} ($X\,^1\Sigma_g^+$), appreciable nonzero FCFs are found to occur for rovibrational levels lying higher than 4600 cm^{-1} above the zero point energy due to the strong change in the equilibrium angle accompanying this transition. For the two other excited states, the calculated spectra consist of long progressions corresponding to both excitations of symmetric stretching and bending modes.

V. DISCUSSION

A. Comparison between the experimental and theoretical spectra

Part (A) of Fig. 2 depicts the double photoionization spectrum of SO_2 at 40.8 eV. We have marked (thick vertical lines) the energy positions of the lowest vibrational levels of $X\,^1\Sigma_g^+$, $a\,^3B_2$ and $A\,^1A_2$ electronic states of SO_2^{++} according to the MRCI T_0 values of Table III, calibrated on the double ionization potential deduced for the $A\,^1A_2$ state. The lower part of Fig. 2 [part (B)] presents a graphical representation of the calculated FCFs listed in Tables V and VI. The first band is assigned to transitions forming the $a\,^3B_2$ state and also the Franck–Condon accessible part of the ground state. The calculated spectrum for $a\,^3B_2$ shown in the lower part of Fig. 2 suggests that most of the intensity of the band is due to this state, probably with some broadening. The second band corresponds to formation of the $1\,^3A_2$ and $1\,^3B_1$ states, which are calculated to lie in this energy range. The third (structured) one is assigned to the $A\,^1A_2$ state. In the lower part of Fig. 2, we show the calculated spectrum assuming an experimental resolution of 45 meV and using the results of Table V (dashed line). We have included only the calculated $SO_2^{++}\,A\,^1A_2\,(v_1,0,0) \leftarrow SO_2\,X\,^1A_1\,(0,0,0)$ transitions (full line) and $SO_2^{++}\,A\,^1A_2\,(v_1,1,0) \leftarrow SO_2\,X\,^1A_1\,(0,0,0)$ transitions (dotted line) (cf. Table VI). Because the Franck–Condon calculations demonstrate that the first strong peak is the (0–0) transition, the adiabatic double ionization potential of SO_2^{++} ($A\,^1A_2$) state is deduced to be 35.284 ± 0.02 eV. By combining this value with our MRCI T_0 values (cf. Table III), we deduce the lowest adiabatic double ionization potential of SO_2 as 33.48 ± 0.1 eV and that of the $a\,^3B_2$ state as 33.03 ± 0.1 eV.

Good agreement is seen between the measured and the calculated spectra for the A state, confirming excitation of the symmetric stretching and bending modes during its formation from SO_2 ($X\,^1A_1$). For the $a\,^3B_2$ band, the global shape of the calculated and measured spectra are similar. However, the experimental spectrum does not show any structures as expected by calculations assuming the same experimental resolution as for the A band. This is probably due partly to the presence of the underlying ground state band

and partly to lifetime broadening from more rapid predissociation of the $a\,^3B_2$ state than of the $A\,^1A_2$ state. The SO_2^{++} $(X\,^1\Sigma_g^+)$ ground state (at least its lower vibrational levels) seems not to be populated in the experimental spectrum, which agrees well with the near zero FCFs calculated for the levels located lower than 0.5 eV above the ZPE of this state. The higher levels will probably contribute a dense manifold of unresolved lines from the bending vibrations underlying the $a\,^3B_2$ band. The many states expected to exist at higher energies, but unresolved in the experimental spectra, are thought to be responsible for the background intensity continuing to high energy in Figs. 1 and 2.

B. Metastability of the lowest excited states of SO_2^{++}

We concentrate in this section on the possible predissociation mechanisms of the electronic states of Fig. 2. For the other states, where they might otherwise be resolved, rapid dissociation (or at least rapid coherence loss) may be happening. It is experimentally established that the great majority of the states dissociate within a few ns, so some coupling to an output channel must exist. Indeed, several repulsive states must cross the relatively bound states and be coupled to them by spin–orbit, Coriolis interactions or BO breakdown. We expect that the singlet states will be less strongly coupled than the triplets according to our analysis for the $a\,^3B_2$ and the $A\,^1A_2$ states (see below). At higher energies the density of states increases so the dissociation rate should rise

For linear configurations, the $i\langle X\,^1\Sigma_g^+, m_s=0|\mathbf{LS}|^3\Sigma^-, m_s=1\rangle$ integral gives no contribution for $\Delta m_s=1$, but for bent structures this selection rule is relaxed and the corresponding integral $(i\langle 1\,^1A', m_s=0|\mathbf{L_xS_x}|1\,^3A'', m_s=1\rangle)$ becomes non zero. The crossing between the $1\,^1A'$ $(X\,^1\Sigma_g^+)$ and the $1\,^3A''$ $(^3\Sigma^-)$ is located in energy >0.5 eV [cf. Figs. 8(a) and 8(b)]. Hence, the vibrational levels of SO_2^{++} $(X\,^1\Sigma_g^+)<0.5$ eV (not observed here due to the near zero FCFs) are predicted to be stable. At the crossing the $i\langle 1\,^1A', m_s=0|\mathbf{L_xS_x}|1\,^3A'', m_s=1\rangle$ integral is calculated to be ~ -18.6 cm^{-1} (for $R_{SO}\sim 3.0$ bohr and for $\theta=118°$) and it should be enough for predissociation of the vibrational levels of SO_2^{++} $(X\,^1\Sigma_g^+)>0.5$ eV to occur. Another mechanism may participate in the predissociation of these levels involving the $1\,^3A'$ (or $a\,^3B_2$) state, which crosses the $1\,^1A'$ at $R_{SO}\sim 2.55$ bohr [for $\theta=118°$, cf. Fig. 8(b)]. At the crossing, the $i\langle 1\,^3A', m_s=1|\mathbf{L_yS_y}|1\,^1A', m_s=0\rangle$ integral is evaluated to be ~ 46.4 cm^{-1}. Then, the second electronic state can be predissociated by the $1\,^3A''$ state for which the $i\langle 1\,^3A'', m_s=1|\mathbf{L_zS_z}|1\,^3A', m_s=1\rangle$ integral is calculated to be ~ 16.6 cm^{-1} at the crossing between these two electronic states [cf. Fig. 8(b)].

The TOF–PEPECO bands of the SO_2^{++} $(a\,^3B_2)$ state are unresolved and are assumed to be wider than the experimental resolution due to lifetime broadening. Such an effect can be rationalized by fast predissociation, for instance, by direct spin–orbit interaction between the $a\,^3B_2$ $(1\,^3A')$ and the $^3\Sigma^-$ $(1\,^3A'')$ for bent geometries. The spin–orbit $i\langle 1\,^3A'', m_s=1|\mathbf{L_zS_z}|1\,^3A', m_s=1\rangle$ integral, which is calculated to be ~ 16.6 cm^{-1} at the crossing between these two

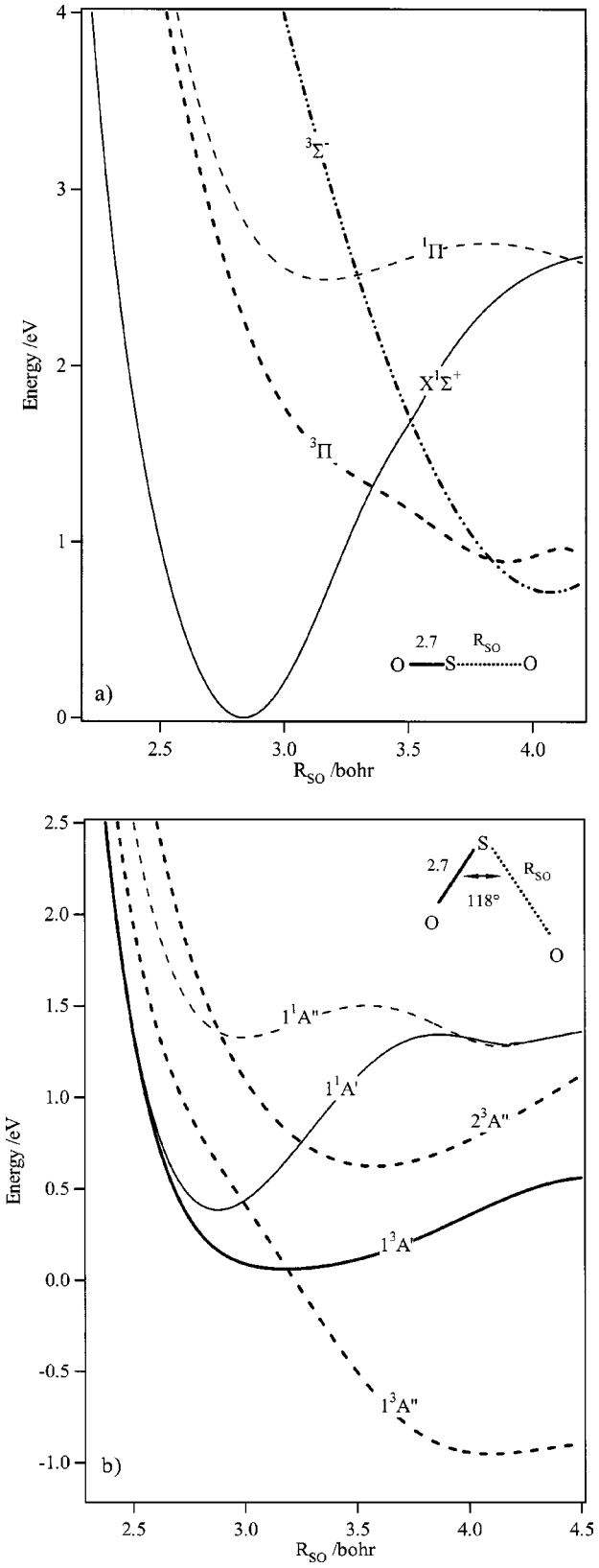

FIG. 8. Interaction between the triplets and the singlets along the R_{SO} distance for linear (a) and bent (b) structures. The other R_{SO} distance is kept fixed to 2.7 bohr.

electronic states [cf. Fig. 8(b)], should be high enough to allow such a reaction. The TOF–PEPECO bands of the $1\,^3B_1$ and $1\,^3A_2$ states similarly exhibit no discernible structures, probably also due to lifetime broadening by predisso-

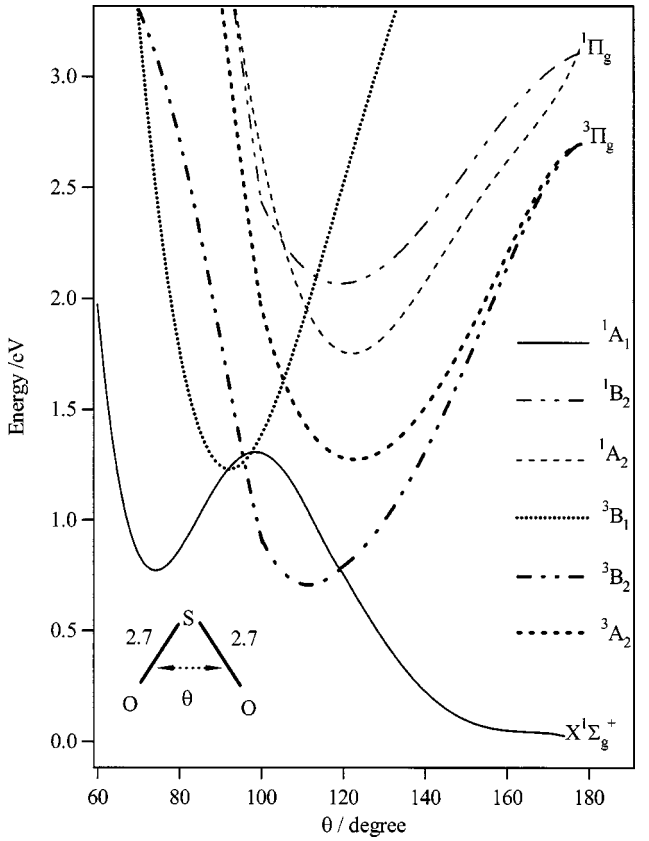

FIG. 9. Interaction between the triplets and the singlets along the bending angle θ.

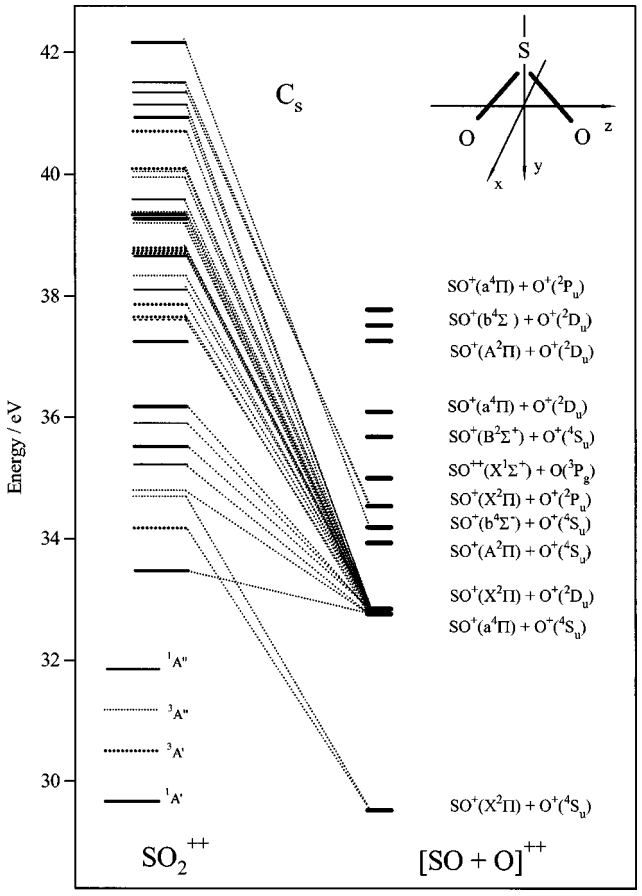

FIG. 10. Schematic correlation diagram for the dissociation of SO_2^{++} into $[SO+O]^{++}$.

ciation processes. The following predissociation pathway can be proposed: after vibronic interaction via the conical intersection (cf. Fig. 9), the $2\,^3A''\,(1\,^3B_1)$ and/or the $A\,^3A_2$ states can be predissociated by the $1\,^1A'$ state which leads to the formation of SO^+ and O^+ as detailed in the previous paragraph. Here again, the spin–orbit integrals are found to be high enough to allow such process. Concerning the $A\,^1A_2$ state, it can be predissociated first by the $1\,^3B_1$ state for bent structures (the $i\langle 2\,^3A'', m_s=1|\mathbf{L}_y\mathbf{S}_y|1\,^1A'', m_s=0\rangle$ integral is calculated to be -45.4 cm^{-1} for $R_{SO}\sim 2.9$ bohr and $\theta=118°$). Then the predissociation mechanisms proposed above for the state $1\,^1B_1$ will lead to the dissociation asymptote. The direct predissociation process for the $a\,^3B_2$ state may account for the faster predissociation of this electronic state than the multistep process found for $A\,^1A_2$.

The experimental results mentioned in the introduction clearly show that most of the dissociation of SO_2^{2+} dications produces ground state products, $O^+(^4S)+SO^+(X\,^2\Pi)$. An adiabatic correlation diagram was produced by Field and Eland[9] using C_{2v} symmetry, but it is very difficult to decipher in published form. Figure 10 depicts a new correlation diagram for the dissociations of SO_2^{++} to the $[SO+O]^{++}$ products. This dissociation most likely occurs in the C_s point group, i.e., for bent structures and when the two SO distances are not stretched symmetrically. In the 28–38 eV energy range, 12 dissociation limits are expected. Figure 10 shows that the electronic states of SO_2^{++} presented in Table I correlate mostly to the three lowest dissociation limits with probably strong vibronic and/or spin–orbit interactions between the PEFs of these electronic states for large R_{SO} distances. The formation of the SO^+ and O^+ products in their ground states (with nonzero internal energy) from electronically excited SO_2^{++} dication may be favorable due to interactions, at long R_{SO} ranges, with the lowest $^3A'$ and $^3A''$ states correlating adiabatically to this limit. The products can also connect to quintet states which have not been calculated in this work, but which we expect to be repulsive and also possibly implicated in the dissociation mechanism.

VI. CONCLUSION

The SO_2^{2+} dication has a dense manifold of electronic states with rather short lifetimes to predissociation, and despite being the first dication to be studied by coincidence methods,[3] it has hitherto escaped detailed spectroscopic examination. The experimental observation of a resolved band together with reliable high accuracy electronic structure calculations has now allowed quantitative analysis of its spectrum. The results largely confirm earlier experimental vertical double ionization energies from double charge transfer experiments,[12] and add a prediction that the dication ground state must lie lower than currently measured energies. This prediction should be verifiable by nonvertical double ionization techniques such as charge stripping from the monocation.

[1] R. G. Cooks, D. T. Terwilliger, and J. H. Beynon, J. Chem. Phys. **61**, 1208 (1974).
[2] J. H. D. Eland, Chem. Phys. **294**, 171 (2003).
[3] G. Dujardin, S. Leach, O. Dutuit, P.-M. Guyon, and M. Richard-Viard, Chem. Phys. **88**, 339 (1984).
[4] D. M. Curtis and J. H. D. Eland, Int. J. Mass Spectrom. Ion Processes **63**, 241 (1985).
[5] J. H. D. Eland, Mol. Phys. **61**, 725 (1987).
[6] S. Hsieh and J. H. D. Eland, J. Phys. B **30**, 4515 (1997).
[7] J. H. D. Eland and D. Mathur, Rapid Commun. Mass Spectrom. **5**, 475 (1991).
[8] T. Masuoka, Y. Chung, E.-M. Lee, and J. A. R. Samson, J. Chem. Phys. **109**, 2246 (1998).
[9] T. A. Field and J. H. D. Eland, Int. J. Mass. Spectrom. **192**, 281 (1999).
[10] M. Thompson, P. A. Hewitt, and D. A. Wooliscroft, Anal. Chem. **48**, 1336 (1976).
[11] M. A. Robb, G. Theodorakopoulos, and I. G. Csizmadia, Chem. Phys. Lett. **57**, 423 (1978).
[12] I. W. Griffiths, D. E. Parry, and F. M. Harris, Chem. Phys. **238**, 21 (1998).
[13] D. Winkoun, D. Solgadi, and J. P. Flament, Chem. Phys. Lett. **139**, 546 (1987).
[14] J. H. D. Eland, O. Vieuxmaire, T. Kinugawa, P. Lablanquie, R. I. Hall, and F. Penent, Phys. Rev. Lett. **90**, 053003 (2003).
[15] J. H. D. Eland, S. S. Ho, and H. L. Worthington, Chem. Phys. **290**, 27 (2003).
[16] P. J. Knowles and H.-J. Werner, Chem. Phys. Lett. **115**, 259 (1985).
[17] H.-J. Werner and P. J. Knowles, J. Chem. Phys. **89**, 5803 (1988).
[18] P. J. Knowles and H.-J. Werner, Chem. Phys. Lett. **145**, 514 (1988).
[19] C. Hampel, K. A. Peterson, and H.-J. Werner, Chem. Phys. Lett. **190**, 1 (1992).
[20] MOLPRO is a package of *ab initio* programs written by H. J. Werner and P. J. Knowles. Further details at www.tc.bham.ac.uk/molpro
[21] T. H. Dunning, J. Chem. Phys. **90**, 1007 (1989).
[22] M. Hochlaf, G. Chambaud, P. Rosmus, T. Andersen, and H.-J. Werner, J. Chem. Phys. **110**, 11835 (1999).
[23] J. Liu, W. Chen, M. Hochlaf, X. Qian, C. Chang, and C.-Y. Ng, J. Chem. Phys. **118**, 149 (2003).
[24] M. Hochlaf, J. Phys. B **37**, 595 (2004).
[25] J. Senekowitcsh, thesis of the University of Frankfurt, Germany, 1988.
[26] I. M. Mills, in *Molecular Spectroscopy: Modern Research*, edited by K. N. Rao and C. W. Mathews (Academic, New York, 1972).
[27] S. Carter and N. C. Handy, Comput. Phys. Rep. **5**, 117 (1987).
[28] M. Hochlaf, G. Chambaud, and P. Rosmus, J. Chem. Phys. **108**, 4047 (1998).
[29] M. Hochlaf, F. R. Bennett, G. Chambaud, and P. Rosmus, J. Phys. B **31**, 2163 (1998).
[30] G. Herzberg, *Molecular Spectra and Molecular Structure III, Electronic Spectra and Electronic Structure of Polyatomic Molecules* (Krieger, Malabar, 1991).
[31] J. H. D. Eland, P. Lablanquie, M. Lavollée, M. Simon, R. I. Hall, M. Hochlaf, and F. Penent, J. Phys. B **30**, 2177 (1997).